npj | Materials Degradation

www.nature.com/npjmatdeg

ARTICLE OPEN

Nanoporous silica gel structures and evolution from reactive force field-based molecular dynamics simulations

J. M. Rimsza[1] and Jincheng Du[1]

Nanoporous silica-rich gel formed on silicate glass surfaces during dissolution in aqueous environment is critical in elucidating the corrosion mechanisms and the long-term residual dissolution behaviors. Silica gel models were created using two types of methods with reactive force field-based molecular dynamics simulations. The results show that the remnant silica gels created from the ISG bulk structure have a more isolated and closed pore morphology and slightly higher glass network connectivity. This contrasts with the gel structures created by hydrogarnet defect formation that exhibit more connected pore morphologies. The remnant gel structures show lower water diffusivity which was explained by the nano-confinement effect of water molecules due to frequent interactions of water molecules with adjacent silica walls and the more isolated pore morphology in the remnant gel structures. These results reveal the complexity in terms of micro and atomic structures of these silica gels, and both structure features have impact on water transport in the gel layer hence the passivating effect that controls the long-term dissolution behavior of these glasses.

npj Materials Degradation (2018)2:18 ; doi:10.1038/s41529-018-0039-0

INTRODUCTION

Silica gels are hydrated nanoporous silica systems commonly found in the fields of biomaterials, including silicate-based bioactive glasses,[1,2] carbon sequestration,[3,4] liquid chromatography,[5,6] and catalysis.[7,8] Silica gels also form during dissolution and consist of several alteration layers, including a hydrated glass and a crystalline layer.[9,10] Experimental elemental profiles have shown that the alteration layer is deficient in soluble species, including sodium, boron, and calcium but rich in silicon.[9] The silica-rich gel region undergoes constant restructuring, posing challenges to experimental characterization due to the complex amorphous structure and high level of hydration.[11,12] Silica gels may passivate the surface by limiting the diffusion of water molecules to reactive interfaces, resulting decreased silicon diffusion into the surrounding environment.[9,13] Alternatively, densification of the gel due to collapse of silica structure or silica condensation from solution may form a barrier to further dissolution.[14–17] Experimental investigations have attempted to identify the origin of the silica gels and connect structure to the dissolution rate.[11] Originally, silica gels were theorized to form from the precipitation of silica from an oversaturated solution,[18] but studies using isotopically tagged samples indicated that only 1:600 silicon atoms in the gel structure had been deposited through condensation.[11] Additional investigation of alteration layers from isotopic and structural analysis support these findings.[10,19,9] Therefore, the silica gel is not a precipitate but instead the reorganization of the remnant glass structure after removal of the soluble species.[11,20–22]

Additionally, the gel is nanoporous, and the small pore size may limit diffusion by slowing movement of water molecules through the silica gel by formation of frozen or structured water.[11] Structured water has been identified both experimentally[23–28] and computationally[29–32] and is caused by the formation of hydrogen bond networks at the water–silica interface which slows internal diffusion.[33] Previous investigations of structured water focused on the interface between water and flat silica surfaces or in large single pores, without considering the role of the gel structure.[29,34,35] The complexities of the silica gel layer and the resulting effect on water diffusion and dissolution rates makes understanding the structure of silica gels a grand challenge in the field of glass corrosion.

Computational methods provide atomistic insight into the properties of silica gels through the development of atomistic models which allow for structural and kinetic analysis of the system. Direct development of silica gel models is relatively rare, and instead nanoporous silica structures are created and hydrated to form gels. Nanoporous silica models are typically created by removing blocks of atoms from silica, creating highly ordered pore structures that do not represent the complexities of experimental systems.[36–38] Alternatively, nanoporous silica models formed through processes that mimic sol–gel[39,40] or chemical vapor deposition (CVD)[41] methods have been created by classical molecular dynamics (MD) or Monte Carlo simulations. Experiments indicate that gels formed during nuclear waste glass dissolution inherit features of the original silicate network structures after the release of the dissolvable species (Na, B, or Ca) and are followed by relaxation and repolymerization of the silica network,[11] unique from sol–gel or CVD-derived porous silica structures and gels. Computational models of silica gels formed from an initial multicomponent glass composition are rare in the literature, possibly due to the complexity of the multicomponent borosilicate glass system, but these structures will allow for detailed description of the structure and properties of dissolution-based silica gels. Recent development of empirical potentials allows for simulations of these boroaluminosilicate glasses.[42]

Such models require reactive and dissociative water potentials to simulate water–silica interfaces. Early work by Garafolini et al.

[1]Department of Materials Science and Engineering, University of North Texas, Denton, TX, USA
Correspondence: Jincheng Du (du@unt.edu)

Received: 22 December 2017 Revised: 20 April 2018 Accepted: 13 May 2018
Published online: 24 July 2018

introduced a reactive water–silica potential for investigations of hydrated silica systems and interfaces.[43] However, the rigid ion three bodied potential does not distinguish oxygen species in the system, limiting the accuracy of the force field. Further development of reactive force fields (ReaxFF) included parametrization to established water–silica reaction mechanisms which can limit spontaneous water–silica interactions.[44] More recently, a set of bond order-based charge transfer potential in the framework of ReaxFF has been developed and used to study water–silica interfaces.[45] ReaxFF was originally developed by van Duin, Goddard, and coworkers and then reparametrized by Yeon and van Duin to improve the description of water–silica systems.[46–48] ReaxFF describes bond breakage and formation due to the calculation of bonding states based on interatomic distances.[48] The bond order-based potential recalculates the bonding environments at each MD step, allowing for smooth transitions from bonded to unbonded systems. In addition to accurately reproducing complex structural features, the ReaxFF potential has also been used to simulate dynamic properties, such as diffusion.[45] The use of the ReaxFF force field in this work allows for simulation of the dynamic heterogeneous nanoporous silica gel structures.

In this work, atomistic silica gels models are formed from two different protocols, one to mimic multicomponent glass dissolution, to provide a unique avenue to understand how the initial structure of a glass can impact the resulting silica gel, and the other from hydrogarnet defect formation from bulk amorphous silica. Hydrogarnet defect is formed by substituting $4H^+$ with Si^{4+} and is the most prevalent structural defect of water uptake in quartz, the stable crystalline form of SiO_2, under equilibrium conditions, as evidenced from both experimental and theoretical studies.[49,50] This represents one of the first atomistic classical MD models which accounts for remnant silica structures in the development of silica-rich gels, and is critical to the development of silica gel models to understand dissolution processes.

Table 1. System size, composition, and density for de-polymerized silica gel (DSG) and remnant silica gel (RSG) structures

Structure	DSG-400	DSG-600	DSG-800	RSG
Density (g/cm^3)	1.25 ± 0.00	1.57 ± 0.00	1.91 ± 0.00	1.62 ± 0.01
Remaining Si (%)	40.0	60.0	80.0	60.9
Total Si (atoms)	400	600	800	618
Si/O ratio[a]	0.191 ± 0.000	0.290 ± 0.000	0.384 ± 0.005	0.312 ± 0.006

[a]Includes all silicon and oxygen atoms in the system, including oxygen from water molecules

RESULTS AND DISCUSSION

Short-range structure

Silica gels are hydrated nanoporous silica composed of interconnected SiO_4 tetrahedron surrounded by water, with silicon concentration varying between 40–80% in the DSG systems. In comparison the RSG structure is composed of ~60% silicon, with all other network modifiers (boron and aluminum) removed (Table 1). Here, the short-range features of the silica gel models are discussed to highlight differences in water structuring between the two model systems. The composition of the nanoporous silica backbone is consistent between the two methods of gel development (Table 2). The extended Si–O–H bond angle of ~124° compared to experiment is a feature of the ReaxFF force field.[51] A ~4° variation in the Si–O–Si bond angle also occurs, but is within the range of values reported experimentally.[52–54] Some Si–O–Si bond angle variation may be due to the intermediate range structure,[55,56] discussed elsewhere in the manuscript.

Structuring of water inside the gel impacts diffusion and reactivity, and has been suggested as a factor in the protective nature of the alteration layers formed during dissolution. In these models the O_w–H_w–O_w bond angles (Fig. 1a) and O_w–O_w interatomic distances (Fig. 1b) exhibit the most variability with the O_w–H_w (0.97 Å) and H_w–H_w (1.52 Å) interatomic distances and H_w–O_w–H_w bond angles (103°) consistent with experiment. Shorter O_w–O_w bond distances of 2.73 ± 0.02 Å are indicative of interfacial structured water which forms within 10 Å of a surface identified by proton NMR and neutron diffraction.[27,29,57–60] In the DSG systems the O_w–O_w interatomic distances decrease from 2.92 to 2.78 Å with increasing silica concentration, compared to ~2.85 Å in bulk water. The contraction of the O_w–O_w pair distribution function (PDF) for the RSG system is more distinct, with a pre-peak located at ~2.69 Å indicating a unique pore structure of the RSG (Fig. 1b). The pre-peak in the RSG system may indicate that the water is either strongly confined, leading to the pre-peak in the O_w–O_w PDF, or in more open diffusive geometries, creating two separate peaks in the PDF. Similar behavior is seen in partially confined water, with slightly contracted O_w–O_w PDF's and a second peak at ~4.0 Å for confinement between plates 7.4–8.6 Å apart.[61] Further investigation of the complex H-bond networks present in silica gels would be beneficial to understand the role of water confinement in complex geometries.

Table 2. Interatomic distances and bond angles for the silica backbone structure of the de-polymerized silica gel (DSG) and remnant silica gel (RSG) from the peak of the bond angle distribution and pair distribution function with the full-width-half-max in parenthesis

	Interatomic distance (Å)	Bond angle (degree)				
	Si–O	O–O	Si–Si	O–Si–O	Si–O–Si	Si–O–H
DSG-400	1.58 (0.14)	2.59 (0.31)	3.09 (0.16)	109 (17)	155 (29)	124 (11)
DSG-600	1.58 (0.15)	2.60 (0.32)	3.10 (0.17)	109 (18)	156 (28)	124 (11)
DSG-800	1.58 (0.14)	2.58 (0.33)	3.10 (0.18)	108 (18)	154 (29)	124 (11
RSG	1.58 (0.11)	2.59 (0.25)	3.11 (0.13)	109 (14)	158 (25)	124 (11)
SiO_2	1.58 (0.11)	2.55 (0.26)	3.06 (0.14)	108 (16)	152 (22)	–
Expt.	1.61[a]	2.65[b]	3.1[c]	109.4[b]	148[d] 153[b]	118.1[e]

[a]Neutron diffraction[93]
[b]Electron diffraction[54]
[c]X-ray scattering[94]
[d]Nuclear magnetic resonance[56]
[e]DFT with 6-31G** Gaussian basis set

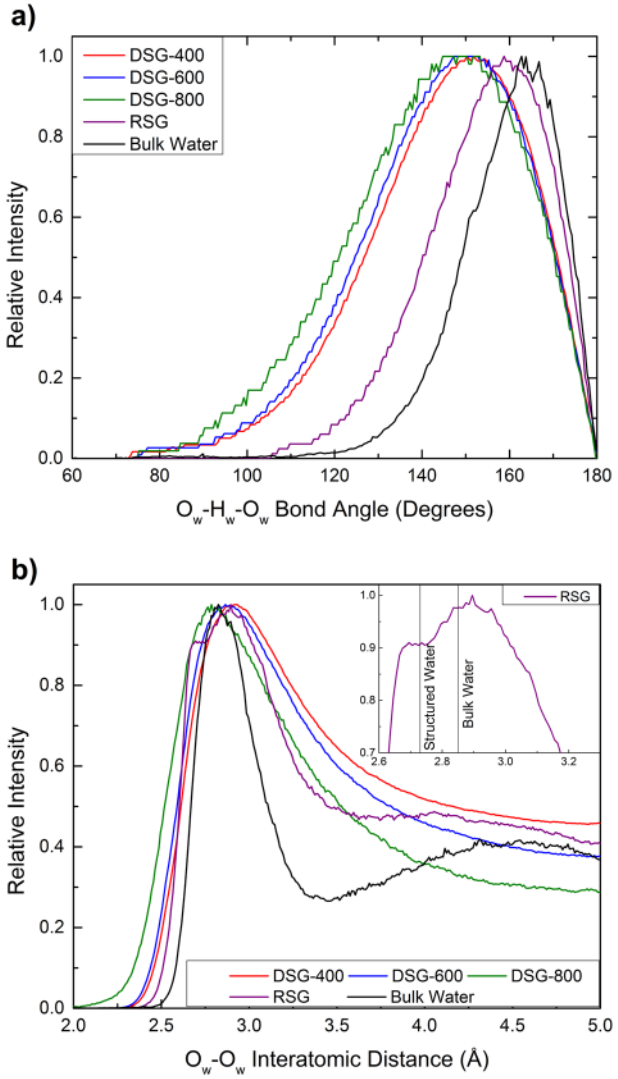

Fig. 1 **a** O_w–H_w–O_w bond angle distribution and **b** O_w–O_w pair distribution function (PDF) for silica gel structures[59]

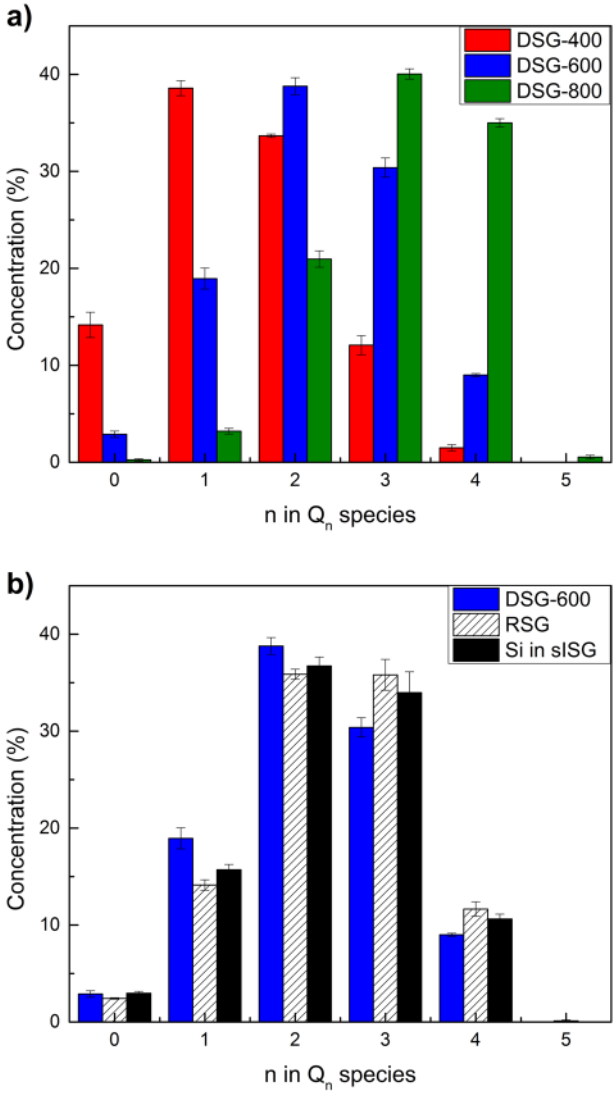

Fig. 2 Q_n distribution of **a** de-polymerized silica gel (DSG) and **b** remnant silica gel (RSG) systems and silica component of the simplified international simple glass (sISG) structure

The O_w–H_w–O_w bond angle is commonly used to identify structured water, with values as low as 139° and as high as 164° depending on the amount of confinement.[61,62] The O_w–H_w–O_w PDF are all contracted by 4–10% compared to bulk water with the RSG system exhibiting an O_w–H_w–O_w PDF peak value only 7° different than bulk water. Decreasing O_w–H_w–O_w angles have been reported for confined water, for example a ~150° O_w–H_w–O_w bond angle for water confined between two planes 6.6 Å apart,[62] providing further evidence for nanoconfined water in complex silica gel systems. The RSG gel structure shows a shoulder of O_w–O_w PDF on the shorter distance (Fig. 1b) and a slightly larger O_w–H_w–O_w bond angle as compared the DSG-400 system (Fig. 1a). This unusual behavior of water in RSG can be related to more isolated pores (as evidenced in the diffusion data reported later), hence higher level of confinement and stronger interaction with the internal pore surface of silica, in RSG gel as compared to other gel structures where more open and connected pores were observed. This is also evidenced by O_w–O_w–H_w bond angle distribution (BAD) (not shown) and enhanced intramolecular hydrogen bonds. This is clearly shown in constrained O_w–O_w interatomic distances in the RSG pre-peak in the spectra (Fig. 1b). No change in the H_w–O_w–H_w bond angle from 104° occurred in any of the simulations, indicating that true hexagonal ice, with a H_w–O_w–H_w bond angle of 109°, is not formed.[63,64] The structuring of the water in the silica gel affects the diffusion coefficient of water in the gel and resulting reactivity, which is discussed in subsequent sections.

Connectivity and intermediate range structures

Connectivity of the silica gel alters its stability and reactivity due to changing activation energies for Si–O bond breakage due to the number of bridging oxygens bonded to the central silicon atom (Q_n distribution with n as the number of bridging oxygen). In the DSG-800 structure, which has the highest silica concentration, the primary Q_n species is a Q_3 which decreases to Q_2 in the DSG-600 and Q_1 in the DSG-400 structure (Fig. 2a). The RSG structure has a broader peak in the Q_n distribution at ~36% for the Q_2 and Q_3 species (Fig. 2b). The similarity in the Q_2 and Q_3 concentration is partially due to the silica remnant of the sISG model, which contains 36.7% Q_2 species and 34.0% Q_3 species (Fig. 2b). The higher Q_3 concentration results in an increased connectivity of 2.40 ± 0.01 compared to 2.24 ± 0.02 for the DSG-600 system with comparable silica concentration. Previous computational investigations have indicated that the Q_2 and Q_3 species in silica are more stable than the Q_1 and Q_4 species,[65,66] and the higher Q_2

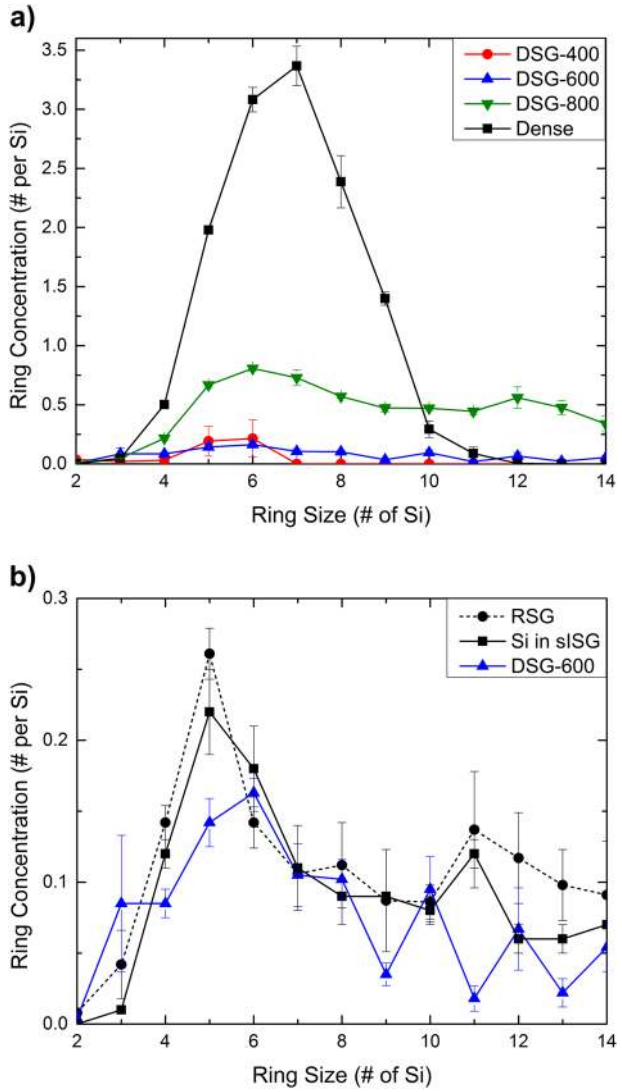

Fig. 3 Ring size distribution of **a** de-polymerized silica gel (DSG) and **b** remnant silica gel (RSG) structures and the silica component of simplified international simple glass (sISG) system

and Q_3 concentrations in the RSG models suggest that the structure would be more stable than comparable DSG systems. An increased concentration of Q_3 species develops in the sISG model, and consequently the RSG structure due to the initial Na^+ concentration which modifies the network through the formation of Q_3 species.[9] Stable concentrations of Q_2 and Q_3 have been reported in experimental silica gels due to retaining Ca^{2+} or Na^+ ions in the glass.[9,67] With additional extended simulations (100 + ns) we hypothesize a complete transition from Q_3 species to Q_4 or Q_2.[9,67] Therefore, the silica gels inherit part of the silica connectivity from the multicomponent glasses structures from which the structures are developed.

Intermediate range structures of glasses are analyzed by the ring size distribution, identified by the number of silicon in a ring, with dense silica composed primarily of seven-membered rings.[53] Peak shifts from seven-membered to six-membered and five-membered rings have been previously identified in nanoporous silica, and continues here (Fig. 3a).[40] The silica ring concentration in the sISG model used as the basis of the RSG identifies that features of the original structure persist into the RSG system (Fig. 3b). In both the RSG and the sISG system five-membered rings exhibit the highest concentration, compared to a six-membered

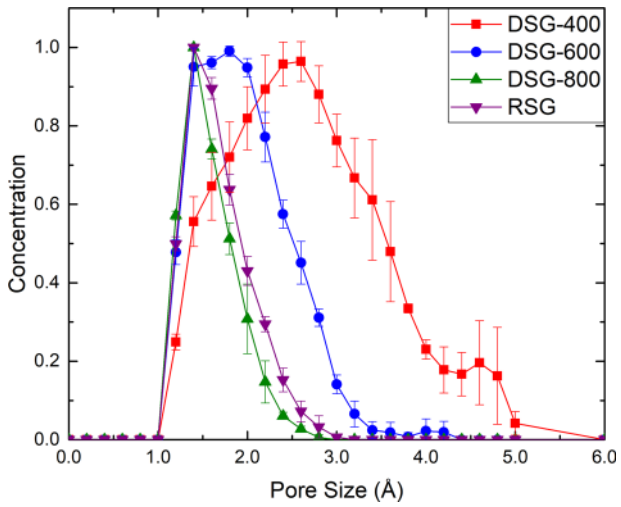

Fig. 4 Normalized pore size distribution in silica gel structures. Error bars are the standard deviation of three different gel structures

ring peak in the DSG-600 system with similar silica concentration. In Fig. 3b the ring size distribution of the silicon atoms in the sISG model indicates a strong five-membered ring peak. Computational silica gel models developed using sol–gel methods identified five-membered rings as an intermediate step in the formation of an interconnected silica network,[68,69] suggesting condensation of the silicon species in the RSG, which is not present in the DSG system. Overall, the RSG system inherits some of the intermediate range order from the multicomponent glass structure, creating a unique structure when compared with DSG systems.

Pore size distributions were also calculated to identify structural differences in the gel between the DSG and RSG systems. The distribution of pore diameters (Fig. 4) inside the system is calculated using the method by Bhattacharya and Gubbins.[70] The DSG-400 model with the lowest concentration of silicon has the broadest distribution of pore sizes with the highest concentration of ~2.5 Å pores. The DSG-600 and RSG systems, which contain the same number of silicon (Table 1) exhibit significantly different pore structures, with the RSG systems having a peak pore size of 1.2 Å in diameter. In comparison, the DSG-600 system has a much broader distribution of pore sizes indicating that the defect formation process creates more connected pores and a more fragmented silica network. This microstructural differences indicates that the pore structure develops differently in systems which begin with either a dense silica gel or a multicomponent oxide. Overall, the intermediate range order of silica gel systems formed from the multicomponent glass structure and depolymerized process are distinct. It is likely that a realistic gel structure would contain features of both DSG and RSG systems. Therefore, the structure of the initial multi-competent glass as well as subsequent dissolution events will develop a gel with features of both systems. Future attempts to create realistic silica gel structures should consider the structure of the original multicomponent glass composition.

Diffusion inside silica gels

Diffusion coefficients of water in the RSG system exhibit typical nanoconfined behavior, with hydrogen diffusion (D_H) rates below bulk water (Table 3). Limited diffusivity may be due to confinement effect due to nanostructured pore features, with water molecules forming H-bond networks adjacent to the surface[71] as suggested by earlier PDF analysis. Due to the complex porosity in the RSG systems most water molecules fall into this interfacial region, resulting in low diffusion coefficients.

Table 3. Diffusion coefficients of hydrogen (D_H) and oxygen (D_O) in the water molecules as well as the silicon (D_{Si}) in the de-polymerized silica gel (DSG) and remnant silica gel (RSG)

	DSG-400	DSG-600	DSG-800	RSG	Water
D_{Si} (10^{-5} cm^2/s)	1.01 ± 0.07	0.07 ± 0.02	0.002 ± 0.002	0.019 ± 0.01	–
D_H (10^{-5} cm^2/s)	6.29 ± 0.26	2.11 ± 0.31	0.39 ± 0.31	0.66 ± 0.29	2.94 ± 0.39
D_H/D_{Si}	6.2	30.1	195.0	34.7	–
Pore size (Å)	2.5 ± 2.3	1.8 ± 1.4	1.2 ± 0.8	1.2 ± 0.9	–
Hydrogen bonds (per Si–OH)	0.50 ± 0.02	0.34 ± 0.01	0.22 ± 0.01	0.20 ± 0.02	–

Furthermore, the pore morphology also plays an important role. Based on the modified random network model of silicate glass structure, there exist modifier cation (e.g., Na^+ and Ca^{2+}) and non-bridging oxygen (NBO, oxygen bond to only one silicon)-rich regions separated from the main Si–O network structure. These regions can form channels and, in compositions like ISG, isolated regions rich in modifier and NBO exist. After dissolution of boron and sodium, the SISG structure leaves behind these isolated pores that are filled with water during the hydroxylation and hydration process. In Figs. 5a and 6a visualization of the water diffusion pathways demonstrate that in the RSG systems the water molecules are trapped inside the pore structure and limited diffusion occurs. It is expected that, after further dissolution of the regions between the confined pores, the pores in the RSG system will become connected. In the DSG systems increasing fragmentation results in D_H values from 6.29×10^{-5} cm^2/s in DSG-400 to 0.39×10^{-5} cm^2/s in the DSG-800 models. D_H values in the DSG-400 system are on the order of bulk water diffusion, indicating the rapid diffusion of water throughout the system. Increased diffusion can be connected with the diffusion of silica, the Q_0 concentration and the hydrogen bond network inside the porous structure.

The highly fragmented nanoporous silica structures (DSG-400) may be developing a water–silica suspension, rather than a stable nanoporous gel through which the water diffuses, leading to high water diffusion coefficients. In these models not only are D_H values elevated in the DSG-400 system, but so are the D_{Si} values, which are between 1.0×10^{-5} cm^2/s to 2.0×10^{-8} cm^2/s, higher than the diffusion coefficient of silicon in silica of 10^{-15} cm^2 (800 K).[72] SiO_4H_4 molecules diffuse at a rate of 2.2×10^{-5} cm^2/s, comparable to the diffusion of silica in the DSG-400 system (Fig. 7a).[73–76] Additional theoretical investigations identify increased diffusion of silica dimer and trimers as well, in comparison to fully connected network silicon.[73] Here, D_{Si} increases with Q_0 concentration approaching the experimental rate for dissolved silica in water in the DSG-400 system.[76] In a stable silica system with water diffusing through the pores a high D_H/D_{Si} value is expected, and in the DSG-800 model the ratio is ~195 (Table 3) indicating the stability of the silica backbone. In the DSG-400 structure the D_H/D_{Si} is 6.2 suggesting that this low-density gel is comparable to a silica–water suspension, with increased water diffusion occurring due to changes in the viscosity and intermolecular forces.[77]

A second compounding factor is the stability of the H-bond network inside the gel.[78] Silanols are predicted to have an H-bond concentration of ~2, with one bond from adsorbed water and the other from adjacent silanols.[79] Calculation of H-bonds contributed by adsorbed water indicates a decreasing concentration from 0.50 ± 0.02 H-bond/silanol in the DSG-400 system to 0.20 ± 0.02 H-bond/silanol in the DSG-800 system (Table 3) indicating an incomplete H-bond network. The RSG system exhibits similarly low concentrations of H-bonds at 0.20 ± 0.02 H-bonds/silanol, below the DSG-600 system with comparable silicon concentrations. The differences in the characteristics of the H-bonds at low concentrations may have an impact on water diffusion through the system, as high H-bond concentrations facilitate water movement by allowing for water hopping through the structure (Fig. 7b). Movement of silica fragments would exacerbate this effect as the H-bond network is continually disrupted, resulting in water diffusion to reform the network. Further investigation of the water network within a highly variable and unordered silica

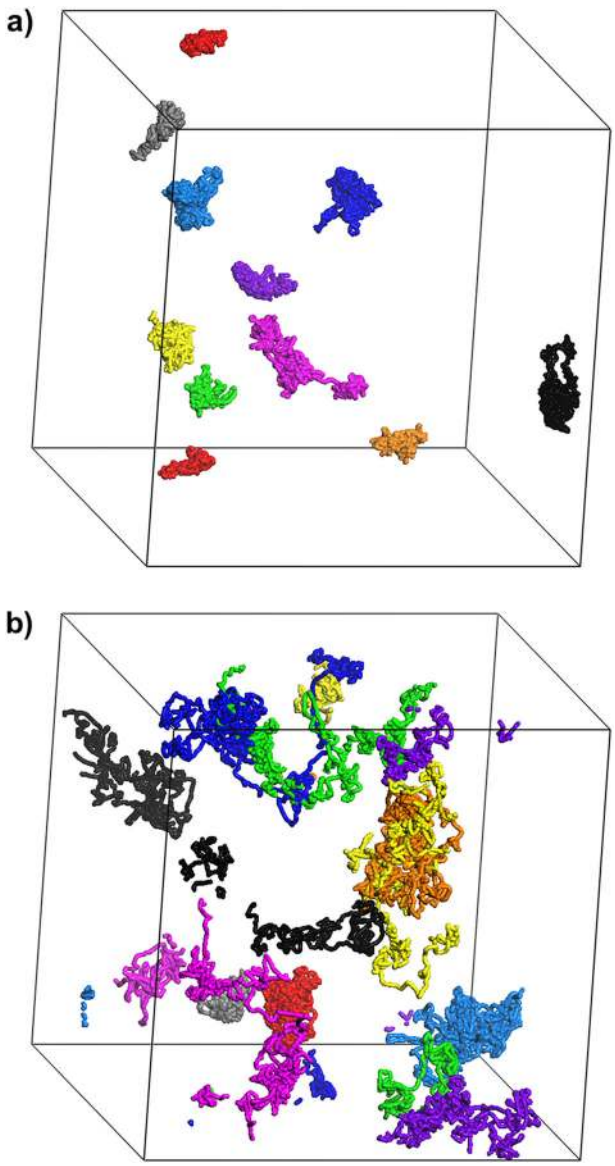

Fig. 5 Diffusion pathways of water molecules in the 50 ps of simulation time at 300 K inside **a** remnant silica gel (RSG) and **b** de-polymerized silica gel (DSG-600) systems. Different colors represent different water molecules

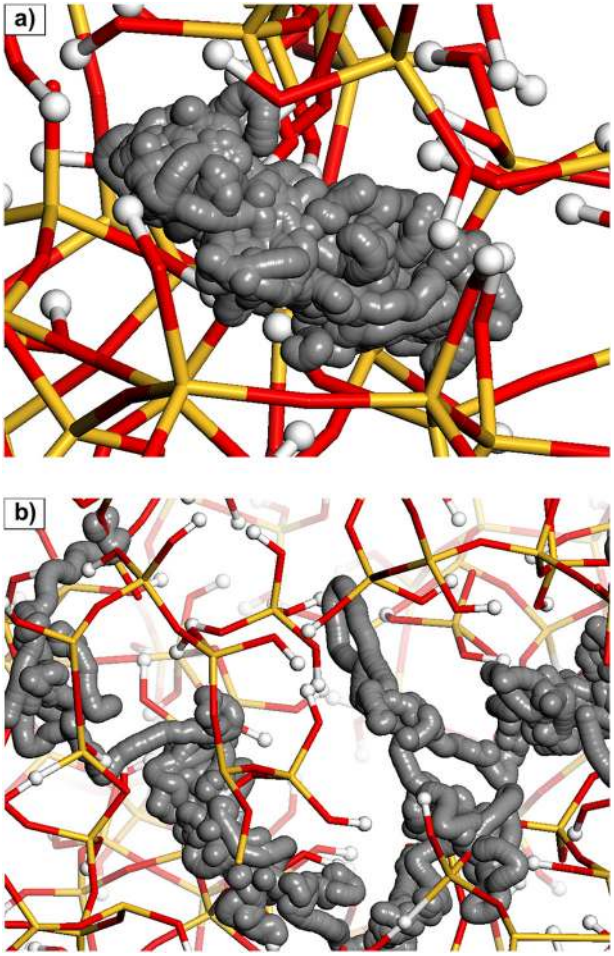

Fig. 6 Snapshots of water diffusion pathways in **a** remnant silica gel (RSG) and **b** the de-polymerized silica gel (DSG-600) system. Colors: Si (yellow), O (red), H (white), diffusion pathway (gray)

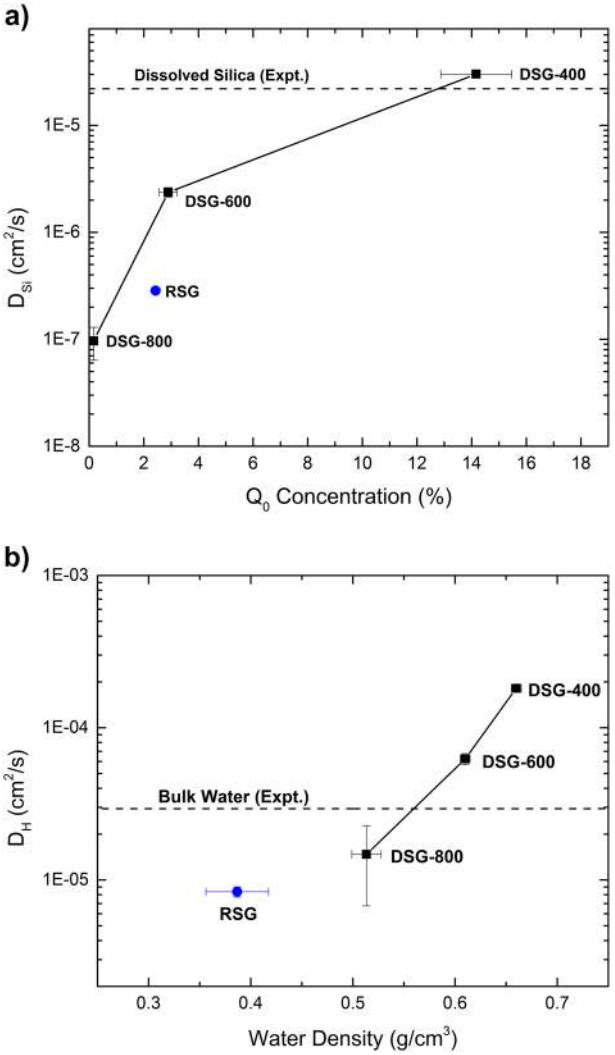

Fig. 7 **a** Silicon diffusion coefficient (D_{Si}) in silica gel structures with Q_0 concentration and **b** hydrogen diffusion (D_H) in water molecules with average hydrogen bond per silanol

structure would provide insight into the effect of H-bond saturation on water diffusion.

Ultimately, the differences in the structure of the silica gel models have an impact on the diffusion coefficients, with the RSG system exhibiting slower diffusion associated with nanoconfinement. Therefore, the underlying framework of the silica in the gel imparted by the original ISG composition creates a more interconnected glass network structure but with more isolated pores, after removing of the dissolvable species, than the randomly created gels. This is reflected in the pore size distribution (Fig. 4) where RSG has narrow pore size distribution as compared to DSG-600, both with similar silica concentration. The DSG-600 and RSG systems also exhibit significantly higher water diffusivity, indicating that the intermediate network structure and pore microstructures are critical in forming an accurate silica gel model which accounts for changing diffusion. Future investigations of silica gels formed on the surface of multicomponent glasses will need to consider the role of the original glass composition when creating realistic structure models, due to the impact on the diffusional properties.

In summary, silica gel models which mimic the interfacial layers formed during the dissolution of silicate glasses in aqueous solutions were created using ReaxFF-based MD simulations. Two different types of models were created, one is the silica remnant of a sodium boroaluminosilicate glass (RSG) and the other one is from dense amorphous silica structure which mimics hydrogarnet defect formation by the random removal of silicon (DSG). The RSG systems exhibit higher concentrations of Q_3 and Q_4 species and five-membered rings due to inheriting the silica network structure in the original multicomponent glass and slight repolymerization after the pore creation. In contrast, the DSG models with comparable silica concentration exhibits lower network connectivity. The remnant gel structures also have smaller pore sizes, narrower pore size distributions, and more isolated pore morphology. Water diffusion coefficients in RSG are significantly lower than in the DSG systems, due to the more isolated pore morphology inherited from the original glass structure and nanoconfinement effect of water molecules due to interaction with the silica walls. In the DSG models the high fragmentation of the silica structure resulted in structures with more open and connected pores, resulting in increased water diffusion. Due to their impact on water diffusivity in these systems, pore morphology and silica network structure are thus critical characteristics for the gel structure development. This work focused on nanoporous silica gel structures and, as other network forming species such as alumina and zirconia also remain in the gel after initial dissolution, their effects on the gel morphology and charge compensating effects remain to be studied.

METHODS

Protocol for silica gel formation

The first method of silica gel formation mimics hydrogarnet defect formation by removing individual silicon from dense silica, since silica dissolves through successive removal of SiO_4 tetrahedral.[65,80] Similar methods were used in silica models of molecular sieves, but did not consider the development of surface silanols (Si–OH) or hydration.[81] A dense silica model was selected for the base structure. To create the 3000 atom model system the parallel MD simulation package DL_POLY was used, with cubic periodic boundary conditions.[82] A partial charge pair wise potential with a long-range columbic interaction and a short-range interaction in the Buckingham form was used, which has been previously applied to silicate glass simulations by Du and Cormack.[83,84] A randomized initial configuration containing 1000 Si atoms and 2000 O atoms was heated to 4000 K and then cooled to 300 K at a rate of 5 K/ps to form a dense silica structure. All other simulations, after the creation of the silica, used the ReaxFF force field.

Hydrogarnet defect formation is the most prevalent form of water update in silica (quartz) under equilibrium conditions[49] and was used to generate the nanoporous silica gel structures. In this method of depolymerization process a silica gel was formed (notation: DSG) by randomly removing silicon atoms forming NBOs which were then terminated with hydrogen to create silanol groups. Of the 1000 silicon atoms present either 20, 40, or 60% were removed to control the connectivity, with the resulting nanoporous silica containing 400 silicon (DSG-400), 600 silicon (DSG-600), or 800 silicon (DSG-800). For hydration a box of water molecules with a density of 1 g/cm^3 was overlaid on the nanoporous silica and water molecules within 1 Å of original system or outside the simulation cell were removed, forming a hydrated silica gel (Fig. 8a). Coordinates for the DSG silica gel structures are included in Supporting Information.

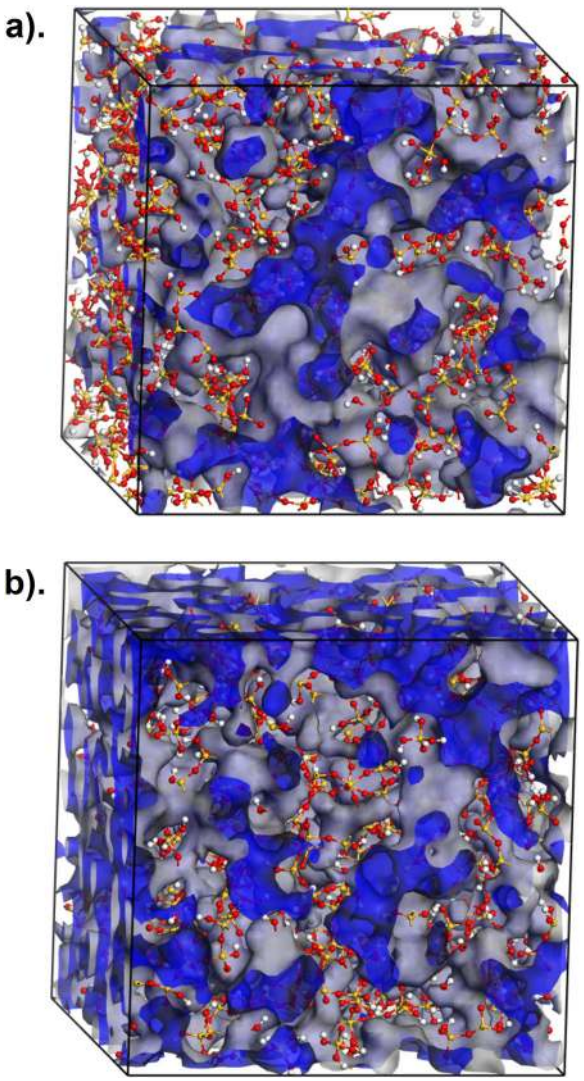

Fig. 8 Snapshots of **a** final DSG-600 structre and **b** final RSG structure. Colors: O (red), Si (yellow), H (white). Interior volume (and water) is represented as a blue and gray isosurface

In the second method the silica remnant of a multicomponent glass structure is used as the base of the silica gel, since dissolution forms interfacial layers by the removal of soluble species.[10,11] Here a simplified international simple glass composition (sISG) was used containing boron, aluminum, silicon, sodium, and low concentrations of CaoO and ZrO_2 (1.7 mole%), incorporated into the Na_2O and SiO_2 components, respectively (Table 4). The simulation of the international simple glass (ISG)[85] composition is not possible with currently available force fields (including ReaxFF), necessitating the simplification of the composition (Table 4). The selected Deng-Du force field[42] has not been parameterized for water–surface interactions, and is therefore only applied in the generation of the multicomponent models. The same multicomponent glass force field has been recently applied in the investigation of ISG glass structures with considerable success.[86]

sISG glass models consisting of ~3000 atoms were created from a melt and quench procedure followed by removal of sodium, boron, and aluminum species.[9,87] During sodium, boron, and aluminum removal NBO defects were formed and then hydrogen terminated to form silanol groups. Extra free oxygen generated during the removal of network modifiers were removed. The nanoporous silica was hydrated by overlaying a box of water molecules on the system and removing overlapping atoms, forming a silica gel (Fig. 8b). Similar methods were implemented for simulation of silica gels from multicomponent glasses by Ohkubo et al.[88] Coordinates for the RSG silica gel structures are included in Supporting Information.

ReaxFF-based MD simulations

Classical MD simulations were performed using the dissociative water–silica potential ReaxFF, developed by van Duin, Goddard, and coworkers and parametrized by Yeon and van Duin.[46–48] ReaxFF accurately simulates bond breakage and formation in water–silica systems due to the identification of bonding states based on interatomic distances.[48] The number of bonds is recalculated between frames, allowing for smooth transitions from bonded to unbonded systems. All of the parameters used to calculate the system energy decrease smoothly with distance, avoiding sudden step-wise changes in energy.[46,48] Here, ReaxFF was implemented in the open source code LAMMPS, a classical MD code distributed by Sandia National Laboratories.[89] After the DSG and RSG systems were created, classical MD simulations using the ReaxFF force field were performed for 100 ps using a 0.25 fs time step for structural relaxation. The temperature (T) was controlled at 300 K through a Nosé-Hoover thermostat with a damping time of 100 time steps. The number (N) of atoms and the simulation volume (V) was also controlled through a canonical (NVT) ensemble.

Analysis methods

Bond distance and angle data were collected from 25,000 snapshots of the silica gel from the last 50 ps of the NVT simulations. BAD and PDF include variations from the amorphous structure and thermal vibrations, and are reported with the peak location and the full-width-half-max values. PDF or BAD peak values were normalized due to the changing number of water

Table 4. International simple glass (ISG) composition and the simplified ISG composition used as the initial conditions for creation of the remnant silica gel (RSG) systems[85]

	Composition (mole %)						Al/B ratio	Density (g/cm^3)
	SiO_2	B_2O_3	Na_2O	Al_2O_3	CaO	ZrO_2		
ISG	60.2	16.0	12.6	3.8	5.7	1.7	0.24	2.50[a]
sISG	61.8	16.0	18.4	3.8	0.0	0.0	0.24	2.49

[a]Archimedes method[95]

molecules in the system. Oxygen atoms in the silica and water were separated for analysis by coordination using a 2.25 Å cut-off. Geometric parameters were also used to identify hydrogen bonds (H-bonds) by using O_w–O_s (oxygen in water and in a silanol group, respectively) distance of less than 3.2 Å and O_s–H_s (hydrogen in a silanol group) distances of less than 2.6 Å. This method is consistent with the interatomic distances used for identification of H-bonds by several previous authors.[90,91]

Diffusion coefficients were calculated from the atomic positions in a 50 ps trajectory recorded every 2 fs. The translational (2D) diffusion is calculated, which considers only atomic movement through the *x*–*y* plane, rather than diffusion of the water molecules in all three dimensions. 2D diffusion was selected to investigate the flux of the atoms through the gel structures. The mean squared displacement was calculated from Eq. (1) with $x_i(0)$ as the position of particle "*i*" at time equal to 0, $x_i(t)$ as the position of the same particle at time equal to *t*, and *n* as the total number of atoms in the system[92]:

$$\mathrm{MSD} = \frac{1}{n}\sum_{i=1}^{n}|x_i(0) - x_i(t)|^2. \quad (1)$$

The Einstein diffusion equation (Eq. (2)) was used for calculation of the diffusion coefficient[92]:

$$D = \frac{1}{6}\lim_{t\to\infty}\frac{\mathrm{d}}{\mathrm{d}t}|x_i(0) - x_i(t)|. \quad (2)$$

Data for hydrogen diffusion was separated into D_H from hydrogen atoms in water molecules (reported here) and hydrogens that are part of silanol groups.

All analysis of the silica gel was performed in triplicate with values reported as the standard error (SE) unless otherwise noted. SE is calculated using Eq. (3), with SD as the standard deviation and *n* as the number of observations/iterations.

$$\mathrm{SE} = \frac{\mathrm{SD}}{\sqrt{n}}. \quad (3)$$

Data availability

The authors declare that all data supporting the findings of this study are available within the paper and its Supplementary Information files.

ACKNOWLEDGEMENTS

Computational resources were provided by UNT's High Performance Computing Services, a division of the University Information Technology with additional support from UNT Office of Research and Economic Development. This work was supported by the Department of Energy Nuclear Energy University Project under Project No. 13-5494 for simulation experiments and analysis and the Center for Performance and Design of Nuclear Waste Forms and Containers, an Energy Frontier Research Center funded by the U.S. DOE, Office of Science, Basic Energy Sciences under Award #DESC0016584 for subsequent data analysis and preparation of this manuscript. J.M. R. also acknowledges that this material was based on work supported by the National Science Foundation Graduate Research Fellowship Program under Grant No. DGE-114248.

AUTHOR CONTRIBUTIONS

J.R. performed the simulations and data analysis. J.D. directed simulation design and data analysis. Both contributed to the manuscript preparation.

ADDITIONAL INFORMATION

Supplementary information accompanies the paper on the *npj Materials Degradation* website (https://doi.org/10.1038/s41529-018-0039-0).

Competing interests: The authors declare no competing interests.

Publisher's note: Springer Nature remains neutral with regard to jurisdictional claims in published maps and institutional affiliations.

REFERENCES

1. Li, P. et al. Apatite formation induced by silica gel in a simulated body fluid. *J. Am. Ceram. Soc.* **75**, 2094–2097 (1992).
2. Cho, S. et al. Dependence of apatite formation on silica gel on its structure: effect of heat treatment. *J. Am. Ceram. Soc.* **78**, 1769–1774 (1995).
3. Adeyemo, A., Kumar, R., Linga, P., Ripmeester, J. & Englezos, P. Capture of carbon dioxide from flue or fuel gas mixtures by clathrate crystallization in a silica gel column. *Int. J. Greenh. Gas Control* **4**, 478–485 (2010).
4. Leal, O., Bolívar, C., Ovalles, C., García, J. J. & Espidel, Y. Reversible adsorption of carbon dioxide on amine surface-bonded silica gel. *Inorg. Chim. Acta* **240**, 183–189 (1995).
5. Siouffi, A. Silica gel-based monoliths prepared by the sol–gel method: facts and figures. *J. Chromatogr. A* **1000**, 801–818 (2003).
6. Nakanishi, K., Minakuchi, H., Soga, N. & Tanaka, N. Double pore silica gel monolith applied to liquid chromatography. *J. Sol Gel Sci. Technol.* **8**, 547–552 (1997).
7. Riego, J. M., Sedin, Z., Zaldívar, J., Marziano, N. C. & Tortato, C. Sulfuric acid on silica-gel: an inexpensive catalyst for aromatic nitration. *Tetrahedron Lett.* **37**, 513–516 (1996).
8. Shi, F., Zhang, Q., Li, D. & Deng, Y. Silica-gel-confined ionic liquids: a new attempt for the development of supported nanoliquid catalysis. *Chem. Eur. J.* **11**, 5279–5288 (2005).
9. Gin, S. et al. Nuclear glass durability: new insight into alteration layer properties. *J. Phys. Chem. C* **115**, 18696–18706 (2011).
10. Ledieu, A., Devreux, F., & Barboux, P. Monte Carlo simulations of borosilicate glass corrosion: predictions for morphology and kinetics. *J. Non Cryst. Solids* **345**, 715–719 (2004).
11. Gin, S. Origin and consequences of silicate glass passivation by surface layers. *Nat. Commun.* **6**, 1–8 (2015).
12. Geisler, T. et al. The mechanism of borosilicate glass corrosion revisited. *Geochim. Cosmochim. Acta* **158**, 112–129 (2015).
13. Gin, S. et al. Atom-probe tomography, TEM and ToF-SIMS study of borosilicate glass alteration rim: a multiscale approach to investigating rate-limiting mechanisms. *Geochim. Cosmochim. Acta* **202**, 57–76 (2017).
14. Cailleteau, C. et al. Insight into silicate-glass corrosion mechanisms. *Nat. Mater.* **7**, 978–983 (2008).
15. Cailleteau, C., Weigel, C., Ledieu, A., Barboux, P. & Devreux, F. On the effect of glass composition in the dissolution of glasses by water. *J. Non Cryst. Solids* **354**, 117–123 (2008).
16. Jollivet, P. et al. Investigation of gel porosity clogging during glass leaching. *J. Non Cryst. Solids* **354**, 4952–4958 (2008).
17. Rebiscoul, D. et al. Morphological evolution of alteration layers formed during nuclear glass alteration: new evidence of a gel as a diffusive barrier. *J. Nucl. Mater.* **326**, 9–18 (2004).
18. Munier, I., Crovisier, J., Grambow, B., Fritz, B. & Clément, A. Modelling the alteration gel composition of simplified borosilicate glasses by precipitation of an ideal solid solution in equilibrium with the leachant. *J. Nucl. Mater.* **324**, 97–115 (2004).
19. Gin, S. et al. The fate of silicon during glass corrosion under alkaline conditions: a mechanistic and kinetic study with the international simple glass. *Geochim. Cosmochim. Acta* **151**, 68–85 (2015).
20. Brinker, C., Kirkpatrick, R., Tallant, D., Bunker, B. & Montez, B. NMR confirmation of strained "defects" in amorphous silica. *J. Non Cryst. Solids* **99**, 418–428 (1988).
21. Casey, W. H., Westrich, H. R., Banfield, J. F., Ferruzzi, G. & Arnold, G. W. Leaching and reconstruction at the surfaces of dissolving chain-silicate minerals. *Nature* **366**, 253–256 (1993).
22. Angeli, F., Charpentier, T., Gin, S. & Petit, J. 17 O 3Q-MAS NMR characterization of a sodium aluminoborosilicate glass and its alteration gel. *Chem. Phys. Lett.* **341**, 23–28 (2001).
23. Gupta, P. K. & Meuwly, M. Dynamics and vibrational spectroscopy of water at hydroxylated silica surfaces. *Faraday Discuss.* **167**, 329–346 (2013).
24. Gouze, B., Cambedouzou, J., Parrès-Maynadié, S. & Rébiscoul, D. How hexagonal mesoporous silica evolves in water on short and long term: role of pore size and silica wall porosity. *Microporous Mesoporous Mater.* **183**, 168–176 (2014).
25. Takamuku, T., Yamagami, M., Wakita, H., Masuda, Y. & Yamaguchi, T. Thermal property, structure, and dynamics of supercooled water in porous silica by calorimetry, neutron scattering, and NMR relaxation. *J. Phys. Chem. B* **101**, 5730–5739 (1997).
26. Li, I., Bandara, J. & Shultz, M. J. Time evolution studies of the H2O/Quartz interface using sum frequency generation, atomic force microscopy, and molecular dynamics. *Langmuir* **20**, 10474–10480 (2004).
27. Pajzderska, A., Bilski, P. & Wąsicki, J. Phase diagram of water confined in MCM-41 Up to 700 MPa. *J. Chem. Phys.* **142**, 084505 (2015).
28. Rosenstihl, M., Kämpf, K., Klameth, F., Sattig, M. & Vogel, M. Dynamics of interfacial water. *J. Non Cryst. Solids* **407**, 449–458 (2015).
29. Bonnaud, P., Coasne, B. & Pellenq, R. J. Molecular simulation of water confined in nanoporous silica. *J. Phys. Condens. Matter* **22**, 284110 (2010).

30. Hou, D., Zhao, T., Ma, H. & Li, Z. Reactive molecular simulation on water confined in the nanopores of the calcium silicate hydrate gel: structure, reactivity, and mechanical properties. *J. Phys. Chem. C* **119**, 1346–1358 (2015).
31. Harrach, M. F., Klameth, F., Drossel, B. & Vogel, M. Effect of the hydroaffinity and topology of pore walls on the structure and dynamics of confined water. *J. Chem. Phys.* **142**, 034703 (2015).
32. Diallo, S. O. Pore-size dependence and characteristics of water diffusion in slit like micropores. *Phys. Rev. E* **92**, 012312 (2015).
33. Sendner, C., Horinek, D., Bocquet, L. & Netz, R. R. Interfacial water at hydrophobic and hydrophilic surfaces: slip, viscosity, and diffusion. *Langmuir* **25**, 10768–10781 (2009).
34. Adeagbo, W. A., Doltsinis, N. L., Klevakina, K. & Renner, J. Transport processes at α-Quartz–water interfaces: insights from first-principles molecular dynamics simulations. *ChemPhysChem* **9**, 994–1002 (2008).
35. Sulpizi, M., Gaigeot, M. & Sprik, M. The silica–water interface: how the silanols determine the surface acidity and modulate the water properties. *J. Chem. Theory Comput.* **8**, 1037–1047 (2012).
36. Roberts, A. P. & Garboczi, E. J. Elastic properties of model porous ceramics. *J. Am. Ceram. Soc.* **83**, 3041–3048 (2000).
37. Coquil, T., Fang, J. & Pilon, L. Molecular dynamics study of the thermal conductivity of amorphous nanoporous silica. *Int. J. Heat Mass Transf.* **54**, 4540–4548 (2011).
38. Miyoshi, H., Hata, N. & Kikkawa, T. Theoretical investigation into effects of pore size and pore position distributions on dielectric constant and elastic modulus of two-dimensional periodic porous silica films. *Jpn. J. Appl. Phys.* **44**, 1166 (2005).
39. Beckers, J. & De Leeuw, S. Molecular dynamics simulation of nanoporous silica. *J. Non Cryst. Solids* **261**, 87–100 (2000).
40. Rimsza, J. & Du, J. Structural and mechanical properties of nanoporous silica. *J. Am. Ceram. Soc.* **97**, 772–781 (2014).
41. Burlakov, V., Briggs, G., Sutton, A. & Tsukahara, Y. Monte Carlo simulation of growth of porous SiO X by vapor deposition. *Phys. Rev. Lett.* **86**, 3052 (2001).
42. Deng, L. & Du, J. Development of effective empirical potentials for molecular dynamics simulations of the structures and properties of boroaluminosilicate glasses. *J. Non Cryst. Solids* **453**, 177–194 (2016).
43. Feuston, B. & Garofalini, S. Empirical three-body potential for vitreous silica. *J. Chem. Phys.* **89**, 5818 (1988).
44. Levine, S. & Garofalini, S. H. A structural analysis of the vitreous silica surface via a molecular dynamics computer simulation. *J. Chem. Phys.* **86**, 2997 (1987).
45. Fogarty, J. C., Aktulga, H. M., Grama, A. Y., Van Duin, A. C. & Pandit, S. A. A reactive molecular dynamics simulation of the silica-water interface. *J. Chem. Phys.* **132**, 174704 (2010).
46. Yeon, J., & van Duin, A. C. ReaxFF molecular dynamics simulations of hydroxylation kinetics for amorphous and nano-silica structure, and its relations with atomic strain energy. *J. Phys. Chem. C* **120**, 305–317 (2015).
47. Van Duin, A. C., Dasgupta, S., Lorant, F. & Goddard, W. A. ReaxFF: a reactive force field for hydrocarbons. *J. Phys. Chem. A* **105**, 9396–9409 (2001).
48. Van Duin, A. C. et al. ReaxFFSiO reactive force field for silicon and silicon oxide systems. *J. Phys. Chem. A* **107**, 3803–3811 (2003).
49. McConnell, J., Lin, J. & Heine, V. The solubility of [4H] Si defects in A-Quartz and their role in the formation of molecular water and related weakening on heating. *Phys. Chem. Miner.* **22**, 357–366 (1995).
50. Lin, J., Payne, M., Heine, V. & McConnell, J. Ab initio calculations on (OH) 4 defects in A-Quartz. *Phys. Chem. Miner.* **21**, 150–155 (1994).
51. Rimsza, J., Yeon, J., van Duin, A. & Du, J. Water interactions with nanoporous silica: comparison of ReaxFF and ab initio based molecular dynamics simulations. *J. Phys. Chem. C* **120**, 24803–24816 (2016).
52. Campbell, T. et al. Structural correlations and mechanical behavior in nanophase silica glasses. *Phys. Rev. Lett.* **82**, 4018–4021 (1999).
53. Yuan, X. & Cormack, A. Efficient algorithm for primitive ring statistics in topological networks. *Comput. Mater. Sci.* **24**, 343–360 (2002).
54. Mozzi, R. & Warren, B. The structure of vitreous silica. *J. Appl. Crystallogr.* **2**, 164–172 (1969).
55. Rimsza, J., Deng, L. & Du, J. Molecular dynamics simulations of nanoporous organosilicate glasses using reactive force field (ReaxFF). *J. Non Cryst. Solids* **431**, 103–111 (2016).
56. Charpentier, T., Kroll, P. & Mauri, F. First-principles nuclear magnetic resonance structural analysis of vitreous silica. *J. Phys. Chem. C* **113**, 7917–7929 (2009).
57. Kinney, D. R., Chuang, I. S. & Maciel, G. E. Water and the silica surface as studied by variable-temperature high-resolution proton NMR. *J. Am. Chem. Soc.* **115**, 6786–6794 (1993).
58. Gallo, P., Rovere, M. & Spohr, E. Glass transition and layering effects in confined water: a computer simulation study. *J. Chem. Phys.* **113**, 11324–11335 (2000).
59. Koga, K., Zeng, X. C. & Tanaka, H. Freezing of confined water: a bilayer ice phase in hydrophobic nanopores. *Phys. Rev. Lett.* **79**, 5262 (1997).
60. Stillinger, F. H. Water revisited. *Science* **209**, 451–457 (1980).
61. Zangi, R. Water confined to a slab geometry: a review of recent computer simulation studies. *J. Phys. Condens. Matter* **16**, S5371 (2004).
62. Zangi, R. & Mark, A. E. Bilayer ice and alternate liquid phases of confined water. *J. Chem. Phys.* **119**, 1694–1700 (2003).
63. Chaplin, M. A proposal for the structuring of water. *Biophys. Chem.* **83**, 211–221 (2000).
64. Kuhs, W. & Lehmann, M. The structure of the ice Ih by neutron diffraction. *J. Phys. Chem.* **87**, 4312–4313 (1983).
65. Kagan, M., Lockwood, G. K. & Garofalini, S. H. Reactive simulations of the activation barrier to dissolution of amorphous silica in water. *Phys. Chem. Chem. Phys.* **16**, 9294–9301 (2014).
66. Criscenti, L. J., Kubicki, J. D. & Brantley, S. L. Silicate glass and mineral dissolution: calculated reaction paths and activation energies for hydrolysis of a Q3 Si by H3O using ab initio methods. *J. Phys. Chem. A* **110**, 198–206 (2006).
67. Robinet, L., Coupry, C., Eremin, K. & Hall, C. Raman investigation of the structural changes during alteration of historic glasses by organic pollutants. *J. Raman Spectrosc.* **37**, 1278–1286 (2006).
68. Rao, N. Z. & Gelb, L. D. Molecular dynamics simulations of the polymerization of aqueous silicic acid and analysis of the effects of concentration on silica polymorph distributions, growth mechanisms, and reaction kinetics. *J. Phys. Chem. B* **108**, 12418–12428 (2004).
69. Garofalini, S. H. & Martin, G. Molecular simulations of the polymerization of silicic acid molecules and network formation. *J. Phys. Chem.* **98**, 1311–1316 (1994).
70. Bhattacharya, S. & Gubbins, K. E. Fast method for computing pore size distributions of model materials. *Langmuir* **22**, 7726–7731 (2006).
71. Faux, D. et al. Model for the interpretation of nuclear magnetic resonance relaxometry of hydrated porous silicate materials. *Phys. Rev. E* **91**, 032311 (2015).
72. Schaeffer, H. A. Oxygen and silicon diffusion-controlled processes in vitreous silica. *J. Non Cryst. Solids* **38**, 545–550 (1980).
73. Doltsinis, N., Burchard, M., Maresch, W., Boese, A. & Fockenberg, T. Ab initio molecular dynamics study of dissolved SiO2 in supercritical water. *J. Theor. Comput. Chem.* **6**, 49–62 (2007).
74. Zotov, N. & Keppler, H. Silica speciation in aqueous fluids at high pressures and high temperatures. *Chem. Geol.* **184**, 71–82 (2002).
75. Zotov, N. & Keppler, H. Letters. In-situ Raman spectra of dissolved silica species in aqueous fluids to 900 °C and 14 Kbar. *Am. Mineral.* **85**, 600–603 (2000).
76. Applin, K. R. The diffusion of dissolved silica in dilute aqueous solution. *Geochim. Cosmochim. Acta* **51**, 2147–2151 (1987).
77. Foss, D. R. & Brady, J. F. Structure, diffusion and rheology of brownian suspensions by stokesian dynamics simulation. *J. Fluid Mech.* **407**, 167–200 (2000).
78. Han, S., Kumar, P. & Stanley, H. E. Absence of a diffusion anomaly of water in the direction perpendicular to hydrophobic nanoconfining walls. *Phys. Rev. E* **77**, 030201 (2008).
79. Lee, S. H. & Rossky, P. J. A comparison of the structure and dynamics of liquid water at hydrophobic and hydrophilic surfaces—a molecular dynamics simulation study. *J. Chem. Phys.* **100**, 3334–3345 (1994).
80. Frugier, P. et al. SON68 nuclear glass dissolution kinetics: current state of knowledge and basis of the new GRAAL model. *J. Nucl. Mater.* **380**, 8–21 (2008).
81. McDermott, T. C. et al. Diffusion within ultrathin, dense nanoporous silica films. *Langmuir* **28**, 506–516 (2011).
82. Forester, T., Smith, W. *The DL_POLY_2 Reference Manual* (Daresbury Laboratory, Daresbury, 2000).
83. Du, J. & Cormack, A. N. Molecular dynamics simulation of the structure and hydroxylation of silica glass surfaces. *J. Am. Ceram. Soc.* **88**, 2532–2539 (2005).
84. Du, J. Molecular dynamics simulations of the structure and properties of low silica yttrium aluminosilicate glasses. *J. Am. Ceram. Soc.* **92**, 87–95 (2009).
85. Gin, S. et al. An international initiative on long-term behavior of high-level nuclear waste glass. *Mater. Today* **16**, 243–248 (2013).
86. Collin, M. et al. Structure of international simple glass and properties of passivating layer formed in circumneutral pH conditions. *npj Mater. Degrad.* **2**, 4 (2018).
87. Gin, S. Open scientific questions about nuclear glass corrosion. *Procedia Mater. Sci.* **7**, 163–171 (2014).
88. Ohkubo, T., Gin, S., Collin, M. & Iwadate, Y. Molecular dynamics simulation of water confinement in disordered aluminosilicate subnanopores. *Sci. Rep.* **8**, 3761 (2018).
89. Plimpton, S. Fast Parallel Algorithms for Short-Range Molecular Dynamics. *J. Comp. Phys* **117**, 1–19 (1995).

90. Shirono, K. & Daiguji, H. Molecular simulation of the phase behavior of water confined in silica nanopores. *J. Phys. Chem. C* **111**, 7938–7946 (2007).
91. Gordillo, M. & Martı, J. Hydrogen bond structure of liquid water confined in nanotubes. *Chem. Phys. Lett.* **329**, 341–345 (2000).
92. Chen, C. & Du, J. Lithium ion diffusion mechanism in lithium lanthanum titanate solid-state electrolytes from atomistic simulations. *J. Am. Ceram. Soc.* **98**, 534–542 (2015).
93. Wright, A. C. Diffraction studies of glass structure. *J. Non Cryst. Solids* **123**, 129–148 (1990).
94. Graetsch, H., Mosset, A. & Gies, H. XRD and 29 Si MAS-NMR study on some non-crystalline silica minerals. *J. Non Cryst. Solids* **119**, 173–180 (1990).
95. Guerette, M. & Huang, L. In-Situ Raman and brillouin light scattering study of the international simple glass in response to temperature and pressure. *J. Non Cryst. Solids* **411**, 101–105 (2015).